Chemical Physics Letters 669 (2017) 137–142

Contents lists available at ScienceDirect

Chemical Physics Letters

journal homepage: www.elsevier.com/locate/cplett

Research paper

Rayleigh-Brillouin scattering in SF_6 in the kinetic regime

Yuanqing Wang [a], Yin Yu [a,b], Kun Liang [a,b,*], Wilson Marques Jr. [c], Willem van de Water [d], Wim Ubachs [a]

[a] Department of Physics and Astronomy, LaserLaB, VU University, De Boelelaan 1081, 1081 HV Amsterdam, Netherlands
[b] School of Electronic Information and Communications, Huazhong University of Science and Technology, Wuhan 430074, China
[c] Departamento de Física, Universidade Federal do Paraná, Caixa Postal 10944, 81531-990 Curitiba, Brazil
[d] Physics Department, Eindhoven University of Technology, Postbus 513, 5600 MB Eindhoven, Netherlands

ARTICLE INFO

Article history:
Received 29 November 2016
In final form 15 December 2016
Available online 18 December 2016

Keywords:
Rayleigh-Brillouin scattering
SF_6 gas
Tenti model
Rough-sphere scattering model

ABSTRACT

Rayleigh-Brillouin spectral profiles are measured with a laser-based scatterometry setup for a 90° scattering angle at a high signal-to-noise ratio (r.m.s. noise below 0.15% w.r.t. peak intensity) in sulfurhexafluoride gas for pressures in the range 0.2–5 bar and for a wavelength of $\lambda = 403.0$ nm. The high quality data are compared to a number of light scattering models in order to address the effects of rotational and vibrational relaxation. While the vibrational relaxation rate is so slow that vibration degrees of freedom remain frozen, rotations relax on time scales comparable to those of the density fluctuations. Therefore, the heat capacity, the thermal conductivity and the bulk viscosity are all frequency-dependent transport coefficients. This is relevant for the Tenti model that depends on the values chosen for these transport coefficients. This is not the case for the other two models considered: a kinetic model based on rough-sphere interactions, and a model based on fluctuating hydrodynamics. The deviations with the experiment are similar between the three different models, except for the hydrodynamic model at pressures $p \lesssim 2$ bar. As all models are in line with the ideal gas law, we hypothesize the presence of real gas effects in the measured spectra.

1. Introduction

Quasi-elastic light scattering is a powerful technique for probing collisional dynamics and relaxation phenomena in gases and liquids. Its theory is based in the description of light in terms of electromagnetism by Lord Rayleigh [1], and the scattering process can be explained in terms of fluctuations, either of density or of entropy. Brillouin [2] and Mandelstam [3] explained that collisions of the gaseous particles inducing acoustic modes in the medium will affect the line shape of the scattering spectral profile. Rayleigh-Brillouin (RB) scattering in various gases has been studied since the 1960s [4–8] using the method of spontaneous RB scattering, which will be followed in the present study. Later, alternative methods were developed, such as stimulated gain Brillouin scattering [9], laser-induced gratings [10], coherent RB-scattering [11,12] and superheterodyne optical beating Brillouin spectroscopy [13,14].

At low densities the spectral profile reflects the Maxwellian velocity distribution of the gas particles. At larger pressures density fluctuations also involve collective particle motion: sound. The key parameter is the ratio y of the scattered light wavelength over the mean free path l_{mfp} between collisions. More precisely, the uniformity parameter y is defined in terms of the scattered light wavenumber k_{sc} as $y = 1/k_{\mathrm{sc}}l_{\mathrm{mfp}}$, and taking for the mean free path the kinetic approximation $l_{\mathrm{mfp}} = v_{\mathrm{th}}\eta_s/p$, with the thermal velocity $v_{\mathrm{th}} = (2k_{\mathrm{B}}T/m)^{1/2}$, η_s the shear viscosity, p the pressure, and m the molecular mass. The length of the scattering wavevector is

$$k_{\mathrm{sc}} = \frac{4\pi n}{\lambda}\sin(\theta/2),$$

with λ the wavelength in vacuum, n the refractive index, and θ the scattering angle. At large values of y, the density fluctuations are described by the equations of the continuum regime, the Navier-Stokes equations. At intermediate values of y, $y = \mathcal{O}(1)$, where the mean free path between collisions is comparable to $1/k_{\mathrm{sc}}$, light scattering is in the kinetic regime, and density fluctuations must be described by the Boltzmann equation. Therefore, whether a kinetic or a hydrodynamic approach is needed to explain the scattered light spectrum, not only depends on the density of the gas, but also on the scattered light wavelength, and thus on the scattering geometry.

Light scattering not only depends on the translational modes of motion of a gas, but also on internal degrees of freedom: rotations

* Corresponding author at: School of Electronic Information and Communications, Huazhong University of Science and Technology, Wuhan 430074, China.
E-mail address: liangkun@hust.edu.cn (K. Liang).

http://dx.doi.org/10.1016/j.cplett.2016.12.033
0009-2614/

and vibrations. Each mode of motion has its own relaxation rate. These relaxation frequencies must be compared to a typical frequency of the density fluctuations: the frequency f_s of sound with wavelength equal to the scattered wavelength, $f_s = c_s k_{sc}/2\pi$, with c_s the speed of sound. When f_s is much larger than the relaxation rate of internal degrees of freedom, internal motion remains frozen on the timescale of the density fluctuations, and only translational degrees of freedom remain. Most light scattering experiments involve translations and rotations only, unlike experiments at ultrasound frequencies, where molecular vibrations may come into play.

A kinetic model of scattered light spectra needs information about the collision properties of the gas molecules, which enters the collision integral in the Boltzmann equation. Such information may be based on explicit molecular interaction parameters. In one of the kinetic models discussed in this paper, collisions are between hard rough spheres that can spin, and thus have internal energy. These collisions are parametrized by the hard-sphere radius and the moment of inertia of the spheres. The roughness allows for the exchange between translational and rotational energy.

On the other hand for the well-known Tenti model [15,16], the collision integral is approximated using the known values of the transport coefficients of a gas. Of these transport coefficients, the heat capacity, the heat conductivity and the bulk viscosity depend on the relaxation of internal degrees of freedom.

If transport coefficients are taken as the input of line shape models, it is important to know if the values used should or should not allow for the relaxation of internal degrees of motion. For example, the bulk viscosity of CO_2 used in light scattering with frequencies $f_s = \mathcal{O}(10^9)$ Hz is three orders of magnitude smaller than the one measured at ultrasound frequencies [17,18]. The reason is that the vibrational relaxation time $\tau_{vib} = 6 \times 10^{-6}$ s (for a pressure of 1 bar and scaling with $\propto 1/p$) is comparable to the period of ultrasound, but slow compared to $1/f_s$.

Line shape models that take the transport coefficients of macroscopic gas dynamics as input are attractive because they can be used to measure these transport coefficients at very large frequencies by comparing measured scattered light spectra to models. In this manner we have recently studied Spontaneous Rayleigh-Brillouin scattering-profiles of N_2 [19] and CO_2 [18], while it was also used to describe RB-scattering in air, where air was treated as a mono-molecular species [20,21]. In the same fashion, the bulk viscosity of several polar and non-polar polyatomic gases was studied using Coherent Rayleigh-Brillouin scattering [22]. The bulk viscosity is an effective parameter that quantifies the relaxation of internal degrees of motion in collisions of molecules. Clearly, the bulk viscosity is frequency dependent, and this dependency could be measured as a function of frequency in experiments where light is scattered at different angles.

In this paper we present measurements of Rayleigh scattering involving sulfur hexafluoride (SF_6) molecules. For SF_6 the vibrational relaxation time is $\tau_{vib} = 2.22 \times 10^{-7}$ s, while the rotational relaxation time is $\tau_{rot} = 6 \times 10^{-10}$ s (both values defined for pressures of 1 bar) [23]. In our scattering geometry, the typical Doppler and Brillouin shifts are $f_s = \mathcal{O}(10^9$ Hz) so that the time scale of measured density fluctuations is approximately two orders of magnitude larger than τ_{vib}, but it is of the same order as τ_{rot}. Therefore, vibrational modes of motion can be ignored, and the high-frequency values of the transport coefficients should be chosen. In addition, rotational relaxation may only be partial at the sound frequencies in our experiment.

In this particular case, models that do not depend explicitly on values of the transport coefficients may perform better. In this paper we will compare two such models to measured SF_6 spectra. Marques [24] has designed a kinetic theory based on a rough-sphere interaction model between rotations and translations. As parameters it takes the moment of inertia of the molecule and the momentum relaxation rate $\sigma = \eta_s/p$, with η_s the shear viscosity and p the pressure. It replaces the linearized collision operator with a simple relaxation term $\propto \sigma(f - f_r)$, where the reference distribution function f_r is designed such that collisional transfers of momentum and energy agree with those of the full Boltzmann collision operator. The SF_6 molecule is ideally suited for application of this model as it is nearly spherically symmetric, while with frozen vibrations its heat capacity ratio c_p/c_v is close to 4/3, c_p is the heat capacity at constant pressure and c_v is the heat capacity at constant volume.

The other theory by Hammond and Wiggins [7] is based on fluctuating hydrodynamics, explicitly involves rotational (and vibrational) relaxation, and takes measured relaxation rates, τ_{vib}^{-1} and τ_{rot}^{-1} and as input. In order to accommodate more rarified gases, Burnett terms are added to the continuum equations [7], but the applicability is still restricted to values of the uniformity parameter $y \gtrsim 1$. However, for light scattering off a CH_4 gas at $y = 2.70$, the two models, one kinetic, and the other one hydrodynamic, are hardly distinguishable [24].

The importance of the frequency dependence of the transport coefficients in explaining light scattering spectra of SF_6 was already recognized by Clark et al. [25], who compares experiments at $2 < y < 55$ with continuum models. Lao et al. [5] propose to change rotational specific heats from their zero-frequency value c_{rot} to $c_{rot}/(1 + 2\pi i f_s \tau_{rot})$, which results in a frequency dependence of the thermal conductivity λ_t through Eucken's formula. Weinberg et al. [26] propose transport coefficients which not only depend on frequency, but also on the wavenumber of sound. In general, if the product $2\pi f_s \tau$ is much larger than 1, the internal degrees of freedom, while relaxing on a time scale τ, do not partake in light scattering. For vibrations of SF_6 $2\pi f_s \tau_{vib} \approx 10^3$, while for rotations $2\pi f_s \tau_{rot} \approx 4$, where we used the sound frequency $f_s = 10^9$ Hz.

Using a recently constructed sensitive light scattering setup [27] with operates at 403 nm and a 90° scattering angle we will revisit Clark's experiments, but with a very high signal-to-noise ratio. Much as in Clark et al. [25] we will address the frequency dependence of transport coefficients, but now in the context of both kinetic and hydrodynamic models: (a) a well-known kinetic model [15,16] which takes transport coefficients as input, (b) a kinetic model which takes collision parameters, and (c) a continuum model that uses known relaxation times of the internal degrees of freedom.

2. Experimental

Rayleigh-Brillouin scattering profiles of SF_6 gas were measured with a sensitive RB-scatterometry setup described previously [27]. A cell equipped with Brewster windows is placed inside a folded optical cavity to enhance the circulating power effectively used for inducing RB-scattering to 5 W. The incident laser wavelength was set to $\lambda = 403.00$ nm [21] for which a narrowband transmission bandpass filter (Materion, $T = 90\%$ at $\lambda = 403$ nm and $\Delta\lambda = 1.0$ nm) was available to reject most of the Raman-scattered light. The RB-spectra were recorded by scanning a plano-concave Fabry-Perot interferometer (FPI) by tuning its piezo voltage. The four sub-modes supported in the FPI have a free spectral range of $FSR = 7.498$ GHz, which was calibrated independently by scanning the laser over some 20 full modes of the FPI with mirror spacings of 5 mm. The instrument linewidth was measured by imposing a reference laser beam to the FPI yielding $\delta\nu_{instr} = 126.7 \pm 3.0$ MHz.

An important parameter for comparing the measured RB-profiles with theory is that of the scattering angle θ. A first

determination is obtained by measurements on the geometrical lay-out of the setup, where narrow pinholes are used to determine beam paths (see Fig. 1 in [27]). Subsequently a test RB-scattering measurement was performed for 1 bar of argon. Analysis of the spectrum, on the basis of a Tenti code adapted for argon (including the macroscopic transport coefficients, while neglecting an effect of a bulk viscosity) yielded a value of the scattering angle $\theta = 89.6 \pm 0.29°$. While care was taken to not rearrange the alignment of the setup, this value is used throughout the present study for measuring an analyzing the spectral profiles for SF_6.

RB spectroscopic data were collected by scanning the FPI analyzer in a stepwise fashion at integration times of 1 s for each position. A full spectrum covering typically 40 RB-peaks in 10,000 data points was obtained in some 3 h. The scanning axis was linearized and converted into a frequency scale by computerized interpolation and matching to the FSR value. Finally the consecutive RB-peaks were overlaid and added to an averaged RB-spectrum, following procedures as discussed by Gu et al. [27].

The data collection rate of 7000 counts/s leads to a noise-to-background ratio of 0.15% (w.r.t. peak height) for a typical spectrum recorded at 1 bar. All experiments were conducted at room temperature. Eight measurements (I to VIII) were performed in a sequence of pressures ranging from 0.2 to 5 bar for which conditions and gas transport coefficients listed in Table 1.

Table 1
Values for pressure (P) and temperature (T) for the eight different measurements of RB-scattering in SF_6. In the last column the calculated non-uniformity parameter y is given. Other relevant parameters of the present study are the scattering wavelength $\lambda = 403.00$ nm and the scattering angle $\theta = 89.6°$.

Data	P (bar)	T (°C)	y-parameter
I	0.215	25.59	0.35
II	0.500	23.36	0.82
III	0.754	24.66	1.22
IV	1.002	23.36	1.64
V	2.002	23.36	3.26
VI	3.002	23.87	4.88
VII	4.000	23.87	6.49
VIII	5.017	23.36	8.14

3. Results

The experimental results are shown in Figs. 1 and 2 for the eight different experimental pressure conditions as listed in Table 1. Due to the larger RB-scattering signals at higher gas pressures, some form of normalization must be invoked for a consistent comparison between experiment and model spectra. For this normalization a scale of equal integrated intensity I_{int} over the spectral profile was chosen. As a result the different peak intensities in the eight experimental spectra, as displayed in the top rows of Figs. 1 and 2 reflect the unity integration over the spectral profile. The scaling implies that the large pressure dependence of the RB-scattering of SF_6 [28] is divided out from the experimental data. A comparison is made with the results of various models, which will be detailed below. For this purpose residuals are determined between experimental intensities $I_e(f_i)$ and modelled spectral intensities $I_m(f_i)$, and these are plotted on the same scale of equal integrated intensity in the second, third and fourth rows in Figs. 1 and 2. We note that we compare in the present study the experimental data with physics-based models, not relying on ad hoc mathematical functional formulas [29,30], to describe the scattering profiles.

As a final figure of merit for the comparison between experiment and the models a summed and normalized root-mean-square deviation is quantified for the spectral profile:

$$\Sigma_{\mathrm{nRMS}} = \frac{\sqrt{\frac{1}{N}\sum_{i=1}^{N}[I_e(f_i) - I_m(f_i)]^2}}{I_{\mathrm{int}}} \tag{1}$$

which is again normalized to the integrated area of the spectral profile. Results of such comparisons are displayed in Fig. 3 for the eight different pressure and y-parameter conditions and the three models discussed below.

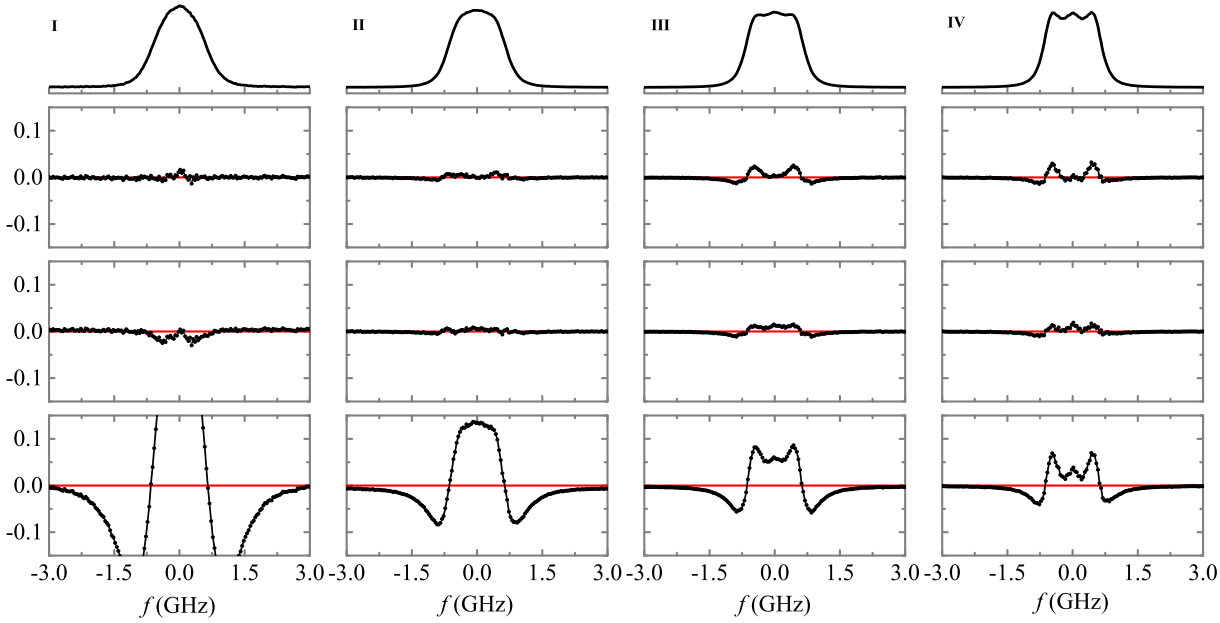

Fig. 1. Data on RB-scattering in SF_6, measured under pressure and temperature conditions as listed in Table 1, indicated by corresponding Roman numerals I-IV, and at $\lambda = 403.00$ nm and $\theta = 89.6°$. Top-line: experimental data on a scale of normalized integrated intensity. Second line: deviations of the Tenti-model (S6) description including a frequency dependence of the thermal conductivity and the bulk viscosity η_b determined from a least-squares fit. Third line: deviations from a rough-spheres model (with $\kappa = 0.227$). In the fourth row, the deviations from the extended hydrodynamic model by Hammond and Wiggins [7] are plotted. Residuals are plotted on a scale of normalized integrated intensity for each profile.

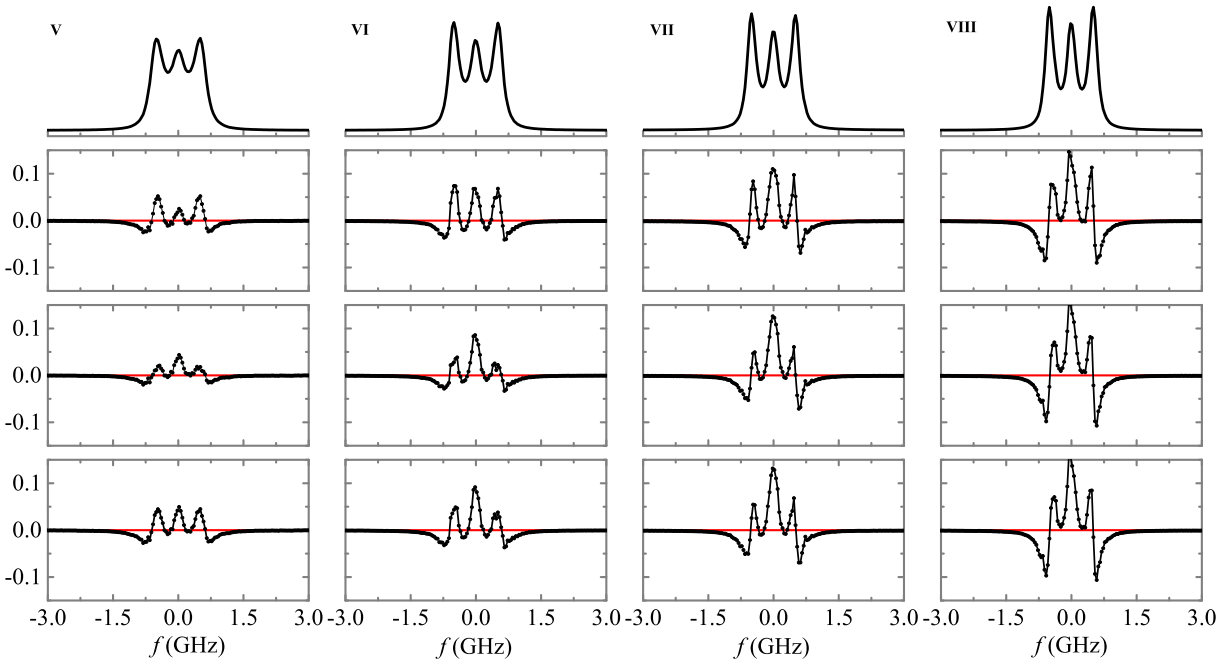

Fig. 2. Continued from Fig. 1 for data sets V-VIII for pressures in the range 2–5 bar. The expression of all the rows are the same as Fig. 1. (Experimental spectra, Tenti S6 model with frequency dependent gas coefficients, rough-sphere model, and the extended hydrodynamic model.)

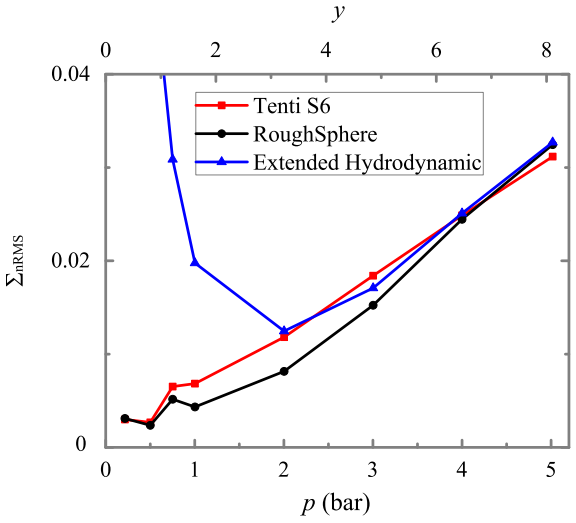

Fig. 3. Normalized root-mean square deviations Σ_{nRMS} as obtained from comparison between experimental spectra and the various line shape models (Tenti-S6, the rough-sphere model, and the extended hydrodynamic model), with data points as indicated in the legend. Along the top axis the dimensionless uniformity parameter y is plotted.

3.1. Comparison with the Tenti model

All models need a value of the shear viscosity, for which we took $\eta_s = 1.52 \times 10^{-5}$ kg m^{-1} s^{-1} [31,32]. For all models we also assumed that vibrations do not partake in the exchange of translational and internal degrees of freedom, and that the molecules are spherically symmetric, so that the heat capacity of internal motion is $c_{int} = 3/2$.

In addition, the Tenti model needs two possibly frequency-dependent transport coefficients as input: the thermal conductivity λ_{th} and the bulk viscosity η_b. The zero-frequency value is $\lambda_{th} = 1.30 \times 10^{-2}$ W m^{-1} K^{-1} [33], but at the GHz frequencies of this light scattering experiment the value should be smaller as vibrational degrees of freedom remain frozen. At these frequencies we estimate the reduction of λ_{th} using Eucken's formula [34]

$$\lambda_{th} = \frac{5}{2}\eta_s c_t/m + \rho D(c_{vib} + c_{rot})/m, \tag{2}$$

where the heat capacities of translations and vibrations are $c_t = c_{rot} = \frac{3}{2}k_B$, and the mass diffusion coefficient is $\rho D = 20.21 \times 10^{-6}$ kg m^{-1} s^{-1}, with ρ the mass density [35]. The heat capacity of vibrations $c_{vib} = 7.66\,k_B$ follows from the heat capacity at room temperature $c_p = 0.664$ J g^{-1} K^{-1} [36], which contains both a rotational and vibrational contribution. The zero-frequency value of λ_{th} is then reduced by the factor $(\frac{5}{2}\eta_s c_t + \rho D c_{rot})/(\frac{5}{2}\eta_s c_t + \rho D(c_{vib} + c_{rot}))$, with the result $\lambda_{th} = 4.72 \times 10^{-3}$ W m^{-1} K^{-1}. In view of the approximate character of Eucken's formula, we ignore a slight pressure dependence of λ_{th} [33].

The kinetic gas model parameters were implemented in an RBS-code for calculating the spectral profiles within a framework of the Tenti model and based on the code by Pan [37]. In the program the bulk viscosity $\eta_b = 1.6 \times 10^{-5}$ kg m^{-1}s^{-1} was determined in a least squares procedure using the $p = 5$ bar data. This value for the bulk viscosity was used in the description of spectral profiles at lower pressures as well. Following a similar procedure as in Vieitez et al. [38], where a value of $\eta_b = 3.5 \times 10^{-5}$ kg m^{-1} s^{-1} was derived. We attribute the changed value to an improved instrument resolution, with respect to the SF_6 measurements in previous experiments [38]. The bulk viscosity $\eta_b = 1.6 \times 10^{-5}$ kg m^{-1} s^{-1} is 300 times smaller than that at low frequencies [39].

The calculated spectral profiles, obtained with the RBS-code for the Tenti-S6 model implementing frequency-dependent transport coefficients and $\eta_b = 1.6 \times 10^{-5}$ kg m^{-1} s^{-1} are convolved with the instrument width and compared with the experimental profiles measured for eight different pressures. Residuals of such comparison are displayed in Figs. 1 and 2.

3.2. Comparison with the rough-sphere model

Apart from the momentum relaxation rate $\sigma = \eta_s/p$, the rough-sphere model needs one additional parameter, the dimensionless moment of inertia κ of the SF_6 molecule, $\kappa = 4I/md^2$, where m, I, and d are the mass, moment of inertia and the effective diameter of the molecule. The rough-sphere model assumes that the spherical surfaces of two colliding molecules have no relative tangential velocity during a collision. This leads to a solvable model for the interaction between translational and rotational motion of the molecules [34]. The moment of inertia I can be assessed directly via spectroscopic investigation of the rotational level structure of SF_6 [40], or via a direct measurement of the bond length R_{SF} via X-ray diffraction [41,42], both yielding a value of $R_{SF} = 1.561$ Å. Via $I = 4M_S R_{SF}^2$ this corresponds to a value of $I = 3.088 \times 10^{-45}$ kg m^2 for the moment of inertia for the SF_6 molecule.

It should be realized that the effective diameter of the SF_6 molecule is not simply $2R_{SF}$ but has a value d which can be determined via experiments on gases. In experiments measuring the viscosity a value of $d = 4.73$ Å was determined [43], which then results in a value of $\kappa = 0.227$. Using the rough-sphere relation between shear- and bulk viscosity, $\eta_b = \eta_s(6 + 13\kappa)/60\kappa$ [34], a value of the bulk viscosity results: $\eta_b = 1.00 \times 10^{-5}$ kg m^{-1} s^{-1}. Alternatively, experiments on molecular sieves and zeolites [44,45] a slightly larger value for the effective diameter of SF_6 molecules was determined, $d = 4.90$ Å, yielding a value of $\kappa = 0.211$ and $\eta_b = 1.05 \times 10^{-5}$ kg m^{-1}s^{-1}. The effect of this difference in effective diameter, resulting in a slightly higher value for the bulk viscosity, was quantified in a model calculation. It results only in a 0.15% difference in peak intensity of the spectral profile, which is negligible.

The formalism used for transforming the rough-sphere model into a RB-scattering spectrum has been described by Marques [24]. Again, the calculated profile was convolved with the instrument function and compared with the experimental data in Figs. 1 and 2, with the normalized root-mean-square deviations of the comparisons presented in Fig. 3.

3.3. Comparison with the hydrodynamic model

Finally, for the hydrodynamic model by Hammond and Wiggins [7] we ignored vibrations, used the rotational relaxation time at $p = 1$ bar, $\tau_{\mathrm{rot}} = 6 \times 10^{-10}$ s, and mass diffusion coefficient $\rho D = 20.21 \times 10^{-6}$ kg m^{-1} s^{-1} [35]. The diffusion of rotational energy D_{rot} was assumed equal to D. The bulk viscosity derived from the rotational relaxation time is $\eta_{\mathrm{b}} = 1.00 \times 10^{-5}$ kg m^{-1} s^{-1} [34], while Eucken's relation leads to a thermal conductivity for translational degrees of freedom $\lambda_{\mathrm{th\,tr}} = 3.25 \times 10^{-3}$ W m^{-1} K^{-1}.

The hydrodynamic model used is the one described by Hammond and Wiggins [7] involving a five-dimensional linear system. It distinguishes kinetic and rotational temperatures, with the associated heat flows. Therefore, it is consistent with a frequency-dependent heat conductivity [7]. This hydrodynamic model evaluates an equation

$$\partial\psi(k_{sc}, t)/\partial t = -M(k_{sc})\psi(k_{sc}, t) \tag{3}$$

where $\psi(k_{sc}, t)$ spans a 5-component vector with as dimensionless elements the Fourier spatial transforms of the fluctuations of mass density $\bar{\rho}/\rho_0$, translational temperature $\overline{T}/T_0$, momentum or velocity density $\bar{v}/v_0$, vibrational temperature $\bar{T}_{\mathrm{vib}}/T_0$, and rotational temperature $\bar{T}_{\mathrm{rot}}/T_0$. The 5×5 coefficient matrix $M(k_{sc})$ involves functions of the transport coefficients [7]. The spectrum of the scattered light is then computed via

$$S(k_{sc}, \omega) = Re[(sI + M(k_{sc}))^{-1}_{11}|_{s=i\omega}] \tag{4}$$

evaluating the real part of the (1,1) matrix element of $\psi(k_{sc}, s)$, which is the Laplacian of $\psi(k_{sc}, t)$. Hence the scattering profile is derived from the density fluctuations in the medium. Via this procedure a model spectrum is calculated, which is then convolved with the instrument width and compared with the experimental spectra in Figs. 1 and 2.

3.4. Difference between experiment and models

The normalized root-mean-square differences Σ_{nRMS} between experiment and the three models introduced and discussed in the above is summarized in Fig. 3. At low pressures, corresponding to $y \lesssim 3$, the hydrodynamic model, understandably, fails. Otherwise the residues of all models with the experiments are very similar: within the experimental accuracy it is impossible to decide in favor for one of the models. This is remarkable as the various models are based on very different physical principles.

However, all models considered share the assumption of SF_6 as an ideal gas. It is well known that scattered light spectra are sensitive to real gas effects, i.e. to the deviation from ideal gas law behavior. The two kinetic models considered in this paper are derived from the linearized Boltzmann equation, which is consistent with the ideal gas law [8]. Similarly, the hydrodynamic model assumes the ideal gas law. We believe that the residual spectra of Figs. 1 and 2 whose amplitudes increase with increasing pressure, point to real gas effects.

4. Conclusion

Light scattering opens a new window on the properties of SF_6 gas, as relaxation phenomena involve rotational degrees of freedom only, while acoustic measurements are dominated by vibrational relaxation. Consequently, the values of the bulk viscosity that we find $\eta_{\mathrm{b}} = (1.0 - 1.6) \times 10^{-5}$ kg m^{-1} s^{-1} are 300 times smaller than those at low frequencies [39]. All three models investigated here to describe the Rayleigh-Brillouin line shape, indicate that the three rotational modes are involved in light scattering.

A surprising finding is the small but significant residues that for $y \gtrsim 3$ are very similar for the three models considered. As the two kinetic models and the hydrodynamic model all assume that SF_6 is an ideal gas, we hypothesize that the deficiency of all models points to real gas effects.

Acknowledgements

Support from the European Space Agency for building the RB-spectrometer is acknowledged. The authors thank Urs Hollenstein (ETH Zürich) for his help during the calibration of the RBS scatterometer. YY, KL and YW thank the Chinese Scholarship Council (CSC) and the Netherlands Universities Foundation for International Cooperation (NUFFIC) for supporting their stay in Amsterdam and VU University for the hospitality. KL, WW, and WU acknowledge the Netherlands Royal Academy of Sciences (KNAW) for funding through the China Exchange Program.

References

[1] J.W. Strutt (Lord Rayleigh), On the transmission of light through an atmosphere containing small particles in suspension, and the origin of the blue of the sky, Philos. Mag. 47 (1899) 375–384.
[2] L. Brillouin, Diffusion de la lumiére et des rayons X par un corps transparent homogéne. Influence de l'agitation thermique, Ann. d. Phys. (Paris) 17 (1922) 88.
[3] L.I. Mandelstam, Light scattering by inhomogeneous media, Zh. Russ. Fiz-Khim. Ova. 58 (1926) 381.

[4] T.J. Greytak, G.B. Benedek, Spectrum of light scattered from thermal fluctuations in gases, Phys. Rev. Lett. 17 (1966) 179.
[5] Q.H. Lao, P.E. Schoen, B. Chu, Rayleigh-Brillouin scattering of gases with internal relaxation, J. Chem. Phys. 64 (1976) 3547.
[6] R.P. Sandoval, R.L. Armstrong, Rayleigh-Brillouin spectra in molecular nitrogen, Phys. Rev. A 13 (1976) 752.
[7] C.M. Hammond, T.A. Wiggins, Rayleigh-Brillouin scattering from methane, J. Chem. Phys. 65 (1976) 2788–2793.
[8] L. Letamendia et al., Light-scattering studies of moderately dense gases. II Nonhydrodynamic regime, Phys. Rev. A 25 (1982) 481.
[9] C.Y. She, G.C. Herring, H. Moosmüller, S.A. Lee, Stimulated Rayleigh-Brillouin gain spectroscopy in pure gases, Phys. Rev. Lett. 51 (1983) 1648–1651.
[10] A. Stampanoni-Panariello, B. Hemmerling, W. Hubschmid, Electrostrictive generation of non-resonant gratings in the gas phase by multimode lasers, Phys. Rev. A 51 (1995) 655–662.
[11] J.H. Grinstead, P.F. Barker, Coherent Rayleigh scattering, Phys. Rev. Lett. 85 (2000) 1222–1225.
[12] X. Pan, M.N. Shneider, R.B. Miles, Coherent Rayleigh-Brillouin scattering, Phys. Rev. Lett. 89 (2002) 183001.
[13] H. Tanaka, T. Sonehara, Superheterodyne light beating spectroscopy for Rayleigh-Brillouin scattering using frequency-tunable lasers, Rev. Sci. Instrum. 73 (2002) 1998–2010.
[14] Y. Minami, T. Yogi, K. Sakai, Rotational relaxation in H_2 gas observed with optical beating Brillouin spectroscopy, J. Appl. Phys. 106 (2009) 113519.
[15] C.D. Boley, R.C. Desai, G. Tenti, Kinetic models and Brillouin scattering in a molecular gas, Can. J. Phys. 50 (1972) 2158.
[16] G. Tenti, C.D. Boley, R.C. Desai, On the kinetic model description of Rayleigh-Brillouin scattering from molecular gases, Can. J. Phys. 52 (1974) 285.
[17] X. Pan, M.N. Shneider, R.B. Miles, Power spectrum of coherent Rayleigh-Brillouin scattering in carbon dioxide, Phys. Rev. A 71 (2005) 045801.
[18] Z. Gu, W. Ubachs, W. van de Water, Rayleigh-Brillouin scattering of carbon dioxide, Opt. Lett. 39 (2014) 3301–3304.
[19] Z. Gu, W. Ubachs, Temperature-dependent bulk viscosity of nitrogen gas determined from spontaneous Rayleigh-Brillouin scattering, Opt. Lett. 38 (2013) 1110.
[20] Z. Gu, B. Witschas, W. van de Water, W. Ubachs, Rayleigh-Brillouin scattering profiles of air at different temperatures and pressures, Appl. Opt. 52 (2013) 4640.
[21] Z.Y. Gu, W. Ubachs, A systematic study of Rayleigh-Brillouin scattering in air, N_2, and O_2 gases, J. Chem. Phys. 141 (2014) 104320.
[22] A.S. Meijer, A.S. de Wijn, M.F.E. Peters, N.J. Dam, W. van de Water, Coherent Rayleigh–Brillouin scattering measurements of bulk viscosity of polar and nonpolar gases, and kinetic theory, J. Chem. Phys. 133 (2010) 164315.
[23] E.U. Haebel, Measurement of the temperature dependence of the oscillation relaxation in sulphur hexafluoride between 10 °C and 215 °C, Acustica 20 (1968) 65.
[24] W. Marques Jr., Light scattering from extended kinetic models: polyatomic ideal gases, Physica A 264 (1999) 40–51.
[25] N.A. Clark, G.R. Mellman, T.J. Greytak, Observation of a frequency-dependent thermal conductivity in a polyatomic gas, Phys. Rev. Lett. 29 (1972) 150–154.
[26] M. Weinberg, R. Kapral, R.C. Desai, Light-scattering experiments and generalized transport coefficients, Phys. Rev. A 7 (1973) 1413–1419.
[27] Z. Gu, M.O. Vieitez, E.J. van Duijn, W. Ubachs, A Rayleigh-Brillouin scattering spectrometer for ultraviolet wavelengths, Rev. Scient. Instrum. 83 (2012) 053112.
[28] M. Sneep, W. Ubachs, Direct measurement of the Rayleigh scattering cross section in various gases, J. Quant. Spectr. Rad. Transfer 92 (2005) 293–310.
[29] B. Witschas, Analytical model for Rayleigh-Brillouin line shapes in air, Appl. Opt. 50 (2011) 267–270.
[30] Y. Ma et al., Analysis of Rayleigh-Brillouin spectral profiles and Brillouin shifts in nitrogen gas and air, Opt. Express 22 (2014) 2092–2104.
[31] R.D. Trengove, W.A. Wakeham, The viscosity of carbon dioxide, methane, and sulfur hexafluoride in the limit of zero density, J. Phys. Chem. Ref. Data 16 (1987) 175–187.
[32] J. Wilhelm, D. Seibt, E. Bich, E. Vogel, E. Hassel, Viscosity measurements on gaseous sulfur hexafluoride, J. Chem. Eng. Data 50 (2005) 896–906.
[33] J. Kestin, N. Imaishi, Thermal conductivity of sulphur hexafluoride, Int. J. Thermophys. 6 (1985) 107–118.
[34] A. Chapman, T.G. Cowling, Mathematical Theory of Non-uniform Gases, third ed., Cambridge Mathematical Library, 1970, ISBN 052140844.
[35] A. Boushehri, J. Bzowski, J. Kestin, E.A. Mason, Equilibrium and transport properties of eleven polyatomic gases at low density, J. Phys. Chem. Ref. Data 16 (1987) 445–466.
[36] C. Guder, W. Wagner, A reference equation of state for the thermodynamic properties of sulfur hexafluoride (SF_6) for temperatures from the melting line to 625 K and pressures up to 150 MPa, J. Phys. Chem. Ref. Data 38 (2009) 33–94.
[37] X. Pan, Coherent Rayleigh-Brillouin Scattering, Princeton University, 2003.
[38] M.O. Vieitez et al., Coherent and spontaneous Rayleigh-Brillouin scattering in atomic and molecular gases, and gas mixtures, Phys. Rev. A 82 (2010) 043836.
[39] M.S. Cramer, Numerical estimates for the bulk viscosity of ideal gases, Phys. Fluids 24 (2012) 066102.
[40] B. Bobin, C.J. Bordé, J. Bordé, C. Bréant, Vibration-rotation molecular constants for the ground and ($v_3 = 1$) states of $^{32}SF_6$ from saturated absorption spectroscopy, J. Mol. Spectr. 121 (1987) 91–127.
[41] V.C. Ewing, L.E. Sutton, Investigation by electron diffraction of the molecular structures of sulphur hexafluoride, sulphur tetrafluoride, selenium hexafluoride and selenium tetrafluoride, Trans. Faraday Soc. 59 (1963) 1241–1247.
[42] L. Bartell, S. Doun, Structures of hexacoordinate compounds of main-group elements: Part III. An electron diffraction study of SF_6, J. Mol. Struct. 43 (1978) 245–249.
[43] J.C. McCoubrey, N.M. Singh, Intermolecular forces in quasi-spherical molecules, Trans. Faraday Soc. 53 (1957) 877–883.
[44] T. Tripp, J. Fox, J. Barney, America, capture & recycle for emission reduction of sulfur hexafluoride in magnesium casting, IMA-Proceedings, vol. 61, International Magnesium Association, 2004, p. 175.
[45] S.P. Koenig, L. Wang, J. Pellegrino, J.S. Bunch, Selective molecular sieving through porous graphene, Nat. Nanotech. 7 (2012) 728–732.